Journal of Magnetic Resonance **154,** 287–297 (2002)
doi:10.1006/jmre.2001.2487, available online at http://www.idealibrary.com on IDEAL®

Evaluation and Comparison of Pulsed and Continuous Wave Radiofrequency Electron Paramagnetic Resonance Techniques for *in Vivo* Detection and Imaging of Free Radicals

Ken-Ichi Yamada, Ramachandran Murugesan,[1] Nallathamby Devasahayam, John A. Cook, James B. Mitchell, Sankaran Subramanian, and Murali C. Krishna[2]

Radiation Biology Branch, Center for Cancer Research, National Cancer Institute, Bethesda, Maryland 20892

Received August 3, 2001; revised November 16, 2001

The performance of two electron paramagnetic resonance (EPR) spectrometers/imagers, one configured in pulsed mode and the other in continuous wave (CW) mode, at an operating frequency of 300 MHz is compared. Using the same resonator (except for altered *Q*-factors), identical samples and filling factors in the two techniques have been evaluated for their potentials and limitations for *in vivo* spectroscopic and imaging applications. The assessment is based on metrics such as sensitivity, spatial and temporal resolution, field of view, image artifacts, viable spin probes, and subjects of study. The spectrometer dead time limits the pulsed technique to samples with long phase memories (>275 ns). Nevertheless, for viable narrow-line spin probes, the pulsed technique offers better sensitivity and temporal resolution. The CW technique, on the other hand, does not restrict the choice at spin probes. In addition, the phase-sensitive narrow-band detection of the CW technique gives artifact-free images even for large objects. Selected examples illustrating the performance of the CW and pulsed techniques are presented to put the capabilities of the two techniques in perspective.

I. INTRODUCTION

In vivo electron paramagnetic resonance (EPR) spectroscopy and imaging studies have recently been carried out in small animals such as mice and rats to obtain information such as tissue redox-status and oxygenation and also to detect free radicals produced in pathological conditions (*1–6*). The sensitivity of EPR spectral properties (hyperfine splitting, linewidth) to physiological parameters such as pH, pO_2, and viscosity makes EPR imaging a potential functional imaging technique (*7*). EPR imaging systems for *in vivo* applications are designed to operate in the low-frequency region (1 GHz–200 MHz), where the dielectric loss is minimal (*8–14*). Most of these efforts have been to develop CW mode techniques to obtain spatial images of spin probe distribution, because of the relatively large linewidths of the commonly used spin probes such as nitroxides or spin adducts. These techniques utilize the inherent advantages of phase-sensitive detection. However, imaging studies using CW techniques require spectral acquisition times in the range 500 ms–10 s (*15*). Additionally, in CW EPR, artifacts associated with sweep rates, magnetic field modulation, power saturation, and physiological motions such as heart beat, peristalsis, and respiration can distort the spectra (*16*).

Pulsed techniques can offer better temporal resolution as well as the Fellgett multichannel advantage for sensitivity enhancement, provided the phase memory of the spin probes is longer than the resonator dead time at the frequencies of operation. With the recently available spin probes exhibiting single narrow lines (*17, 18*), time-domain EPR at radiofrequency (RF) has become a viable technique for *in vivo* applications (*19*). Using these probes, the feasibility of 3D whole-body imaging of small animals by time-domain EPRI at 300 MHz has been demonstrated (*20, 21*). A few other pulsed RF EPR imaging spectrometers with limited temporal resolution have also been reported (*22–24*).

The time-domain EPR method requires the use of narrow-line paramagnetic spin probes. But, as mentioned earlier, spin probes such as nitroxides possess larger linewidths. Hence to study nitroxide, nitric oxide, and other free radicals of biological interest, we have also recently developed a CW RF EPR spectrometer/imager (*8*). In this communication, the technical specifications and performances of our pulsed and CW RF EPR spectrometers/imagers operating at 300 MHz are compared with the aim of identifying the areas of applications where one technique may be more suitable than the other. Comparison of pulsed EPR versus CW-EPR, especially at RF, becomes interesting because of the potential applications and experimental difficulties of each modality employed in detecting paramagnetic species.

[1] On leave from Madurai Kamaraj University, Madurai, India.

[2] To whom correspondence should be addressed at Building 10, Room B3 B69, NIH, Bethesda, MD 20892-1002. E-mail: murali@helix.nih.gov.

1090-7807/02

II. THEORETICAL AND EXPERIMENTAL CONSIDERATIONS

A. Pulsed Method

Spectrometer Dead Time

The performance of a pulsed EPR spectrometer mainly depends upon the spectrometer dead time, excitation bandwidth, and sensitivity (*25, 26*). The dead time of the spectrometer is a critical parameter because it severely affects the choice of spin probes that could be studied by pulsed EPR. Although there are several factors that contribute to the dead time, for low-frequency operation the major source is the ring down-time constant of the resonator, which is given by

$$\tau_r = Q_L/\omega. \quad [1]$$

Here Q_L is the loaded quality factor of the resonator. The dead time, which is inversely related to the carrier frequency ω, poses a serious problem for the successful detection of the time-domain EPR responses at RF. Therefore, unlike EPR at high frequencies, where time-domain responses from nitroxides have been collected using high-Q cavity resonators, detection of EPR signals from fast-relaxing spin probes might not be feasible at RF frequencies. Hence an optimal Q must be selected, based upon the spectral properties of the paramagnetic spin probe under investigation. The parallel coil resonators used in this study have been evaluated for their capability in time-domain EPR spectroscopy and imaging at radiofrequency. To implement the technique in small animal imaging, an optimal Q value of 25 has been selected (*21*). A resonator Q of 25 leads to a time constant, τ_r, of about 13 ns at 300 MHz. The dead time τ_d can be evaluated from the equation

$$\tau_d = \Delta P/d_r, \quad [2]$$

where d_r is the corresponding damping parameter given by

$$d_r = -10\log[\exp(-10^9/\tau_r)]\ \text{dB/ns} \quad [3]$$

and ΔP determines the level to which the power at the receiver input must decay before the receiver can start acquiring the weak free induction decay (FID). For a receiver with a dynamic range of 60 dB, ΔP becomes about 80 dB, resulting in a dead time of about 240 ns. Any further attempt to reduce the dead time by decreasing the Q may compromise the sensitivity significantly. In pulsed EPR spectrometers, Q is generally reduced to the desired value by overcoupling, because for the same RF power, higher B_1 fields could be achieved by overcoupling (*27*). However, in a strongly overcoupled mode, the observed dead time may be longer than the τ_r-limited value because of reflection of the exciting radiation, even though the reflections at low frequencies are not as significant as those in high-frequency spectrometers.

Another factor contributing to the dead time is the recovery of the saturated components in the receive arm. For example, the FID is often seen to grow in the beginning, despite the fact that it should be an exponentially decaying function. This growth occurs during the recovery of the preamplifier. Besides limiting the sensitivity of the spectrometer, the dead time may lead to considerable distortion in the spectral features, if the resulting truncated FID is Fourier transformed without any phase correction (*28, 29*). Several phase correction procedures are routinely used in NMR spectroscopy (*30*). Frequency-dependent phase corrections are made to individual isolated peaks and then frequency-independent phase corrections may be made to bring all the peaks to the absorption mode. This process is iterated to obtain reasonable accuracy. But in imaging, there may not be any well-separated individual peak. For example, in a 1D projection the spins experience a local static field of $B_0 + B(r)$ in the gradient direction (*31*). The acquisition of the FID is not possible until the dead time. But by that time the phase of the magnetization would be

$$\phi(r,\ t) \propto\ \tau_d\,\omega(r). \quad [4]$$

Thus the magnetization components accumulate phase errors in proportion to their observed frequencies (*31*). The missing time interval may be too large for proper data reconstruction at high offset frequencies. Hence the dead time problem becomes more significant in EPR imaging than in NMR imaging. To avoid distortions associated with phase errors in the images, the absolute-value mode spectra of the projections can be computed by Fourier transformation of the experimentally collected FIDs. The linewidths of absolute mode spectra are larger than the widths of the absorption or power mode spectra, causing loss of image resolution. Apart from the reduction in resolution due to the employment of magnitude mode spectral lineshape, there are additional factors that are to be addressed in pulsed EPR imaging. The transverse relaxation (T_2^*) is a function of the overall spread in frequency, in presence of the imaging gradients. For oblong objects the spread in frequency is a function of the gradient orientation and leads to differential dead-time loss. Thus when the gradient is along the longest axis of spin distribution, the increased frequency range may lead to considerable loss in the integrated intensity of the profile, compared to that obtained when the gradient is parallel to the shortest spin distribution dimension. This is further compounded by the Q-profile (the spectral response) of the resonator, which attenuates the spectral density at either extreme of the frequency bandwidth. Added to this is the sinc $((\sin x)/x)$ profile of the power spectrum of the rectangular excitation pulse. These lead to distortions in the image quality for large gradients and in larger objects in the pulsed mode. However, by limiting the magnitude of the gradients and by suitable pulse shaping (using Gaussian or sinc pulses) one can largely eliminate most of these artifacts. Linear prediction methods may be used to correct the FID for the loss of data during the dead time (*32, 33*). But such procedures may not be easy

where one has to deal with continuous spread of frequencies as in EPR imaging. This problem cannot be completely avoided, but the various phase correction algorithms may alleviate it to some extent.

Sensitivity

The sensitivity of a pulsed EPR spectrometer is conveniently described in terms of SNR per unit time (more precisely per $t^{1/2}$). The SNR per $t^{1/2}$ of a signal-averaged free induction decay (FID) is given by (*34–36*)

$$\mathrm{SNR} \propto M_0 E \sqrt{(2MnK)} \exp(-\tau_d / T_2^*), \qquad [5]$$

where M is the number of samples in an FID, n is the number of FIDs averaged, K is the duty cycle of the receiver, τ_d is the spectrometer dead time, and T_2^* is the spin–spin relaxation time of the spin probe. Here M_0 is the static magnetization of the sample and E is the sensitivity factor, given by

$$\begin{aligned} M_0 &= Ng^2\beta^2 S(S+1)B_0/3kT \\ E &= \sqrt{\mu_0 \omega Q_L / 8 V_C \kappa T F_N}. \end{aligned} \qquad [6]$$

Here F_N is the receiver noise figure, N is the spin count, V_C is the volume of the resonator, $\mu_0 = 4\pi \times 10^{-7}$ H m^{-1}, and κ is the Boltzmann constant. Except for the noise factor, which depends upon the bandwidth, the other terms in [6] are common to both CW and pulsed techniques. The large value of the ratio $(-\tau_d / T_2^*)$ compared to NMR makes the loss in sensitivity due to the spectrometer dead time (Eq. [5]) more critical in pulsed RF EPR. Therefore the data sampling and summing capabilities of the spectrometer become very critical for the enhancement of SNR.

Frequency Dependence of the Sensitivity

It is generally conceived that for pulsed spectroscopy at radio frequencies the Boltzman factor and the dead time may dominate to such an extent that it may become prohibitive to obtain any reasonable SNR. Hence it will be of interest to analyze the frequency dependence of sensitivity of pulsed RF EPR (*37*). For constant RF field and excitation bandwidth the SNR may be given by

$$\mathrm{SNR} \propto \omega^{3/2} N Q_L^{1/2} / \left(F_N^{1/2} V_C^{1/2}\right). \qquad [7]$$

In the case of uniform excitation over full bandwidth, using the relation $Q_L \propto \omega / \Delta\nu$ Eq. [7] may be reduced to

$$\mathrm{SNR} \propto \omega^2 N V_C^{-1/2} F_N^{-1/2}$$

and

$$N_{\min} \propto \omega^2 V_C^{1/2} F_N^{1/2}. \qquad [8]$$

Here $N_{\min}$ is the minimum number of detectable spins and, using the relationship between the sample volume V_S, the filling factor η, and the minimum detectable concentration, $(N/V_S)_{\min}$ can be written as

$$(N/V_S)_{\min} \propto \omega^2 \eta^{-1} V_C^{-1/2} F_N^{1/2}. \qquad [9]$$

The ω^2 dependence given Eqs. [8] and [9] is valid for situations where the noise is dominated by the preamplifier noise. But, for lossy *in vivo* samples, the sample noise will be a dominating figure. An elaborate discussion on frequency dependence of EPR signal intensities has been presented recently (*38*).

Different strategies to optimize $N_{\min}$ and $(N/V_S)_{\min}$ at higher frequencies have been described (*25*). Although the sensitivity per unit volume is high, the sample volume becomes limited as the frequency increases. On the other hand, sample size limitation is not a problem at lower frequencies. In fact, the main reason for the selection of RF is its potential for studying large objects. Hence, the possibility of using a large resonator and the high filling factor may compensate to some extent for the frequency-dependent loss in SNR (*37*). Additionally, the SNR degradation by noise is also relatively small at lower frequencies. Thus it is possible to get reasonable sensitivity at lower frequencies by designing suitable large resonators with very high filling factors. But this will depend upon the power available to excite the entire spectrum. Although this could be achieved for the spectroscopy of narrow-line spin probes, it becomes a formidable challenge when imaging of large samples is attempted.

Spectral Excitation Bandwidth

In an FT experiment, following an RF pulse, ideally the magnetization due to all portions of the spectrum must be rotated by an equal angle given by

$$\theta = \gamma_e B_1 t_p. \qquad [10]$$

However, this depends upon the available RF power and the spectral bandwidth. If Δf is the possible spectral range then

$$\gamma B_1 \gg 2\pi \Delta f. \qquad [11]$$

In single pulse experiments, a 90° pulse is applied to achieve the maximum sensitivity and the pulse width should satisfy the condition (*39*)

$$t_p(90^\circ) \ll 1/4\Delta f. \qquad [12]$$

Even for single, narrow-line spin probes, this may pose a problem when imaging of a large object or under a very high gradient is attempted. It has been shown that when the excitation bandwidth $\Delta\nu$ (given by γB_1) is not comparable to the spectral bandwidth Δf, destructive interference between contributions of spins with similar resonance offsets can suppress the signal

intensity (*29*). The phase dispersion of the magnetization that is excited off resonance becomes very significant, resulting in substantial sensitivity loss when the spectral bandwidth exceeds the excitation bandwidth by a factor of 5 or more. However, one can attempt to enhance the excitation bandwidth by increasing the RF power. The RF power available at the resonator, P_0 (in W), is given by

$$P_0 = V_C(2B_{1C})^2\omega/2\mu_0 Q_L, \quad [13]$$

where ω is the resonance frequency (radian s^{-1}), B_C is the maximum amplitude of the circularly polarized component of the RF field (in tesla), and V_C is the resonator volume. Taking into consideration that the half-power full bandwidth of the resonator is given by ω/Q_L, the P_0 dependence on the excitation bandwidth can be seen to be

$$P_0 \propto (\Delta\nu)^3 V_C. \quad [14]$$

This cubic dependence of the required power on the excitation bandwidth can limit the size of the object to be imaged. The high cost of class A, high power amplifiers, the experimental difficulties associated with isolating and protecting the receiver, and the preamp recovery due to the overload from high power excitation pulses set an upper limit on the spectrometer power. These difficulties may to some extent be minimized if a very efficient resonator is designed. The resonator efficiency parameter Λ is defined by

$$\Lambda = B_1/\sqrt{P_0}, \quad [15]$$

where B_1 is the maximum available RF magnetic field for a given incident RF power. A high Λ reduces the energy required per pulse, thereby lessening the technical difficulties associated with the isolation of the high transmit pulse from the receiver. For example, a 10-fold increase in Λ would require 20 dB less RF power to achieve the same B_1 field at the sample (*40*). This in turn would realize an effective 20-dB increase in the transmit–receive isolation. Therefore, high-Λ and low-Q resonators will be the ideal choice for pulsed RF EPR studies.

B. CW Method

In a slow passage experiment, the time dependence of the absorption signal is given by

$$S(t) \propto M_0 E \gamma_e B_1 T_2/\{1 + S' + (2\pi r t T_2)^2\}. \quad [16]$$

Here S' is the saturation factor, $S' = (\gamma_e B_1)^2 T_1 T_2$, and r is the sweep rate in Hz/s. In the absence of saturation, the maximum sensitivity of a CW experiment with matched filtering, expressed in signal-to-noise ratio per unit time, is given by

$$\mathrm{SNR_{CW}} \propto M_0 E \sqrt{(1/(\Delta f T_1))}. \quad [17]$$

It is interesting to note that the achievable signal intensity is independent of T_2 when the experiment is done under nonsaturating conditions. Hence the CW method is well suited when the free radical to be studied has a large linewidth. But, for narrow-line spin probes, caution should be exercised in selecting the RF power.

The selection of the modulation amplitude, B_m, depends upon how much sensitivity can be sacrificed to get distortion-free spectral information (*16*). The modulation amplitude should be also small enough so that the resulting spectrum will be a faithful reproduction of the absorption lineshape. Although increasing the B_m can increase the peak-to-peak height of the CW signal, in imaging experiments distortion-free spectra are essential to get a faithful reproduction of the projections to arrive at accurate spatial as well as spectral parameters. When resolution and true lineshape are of prime concern, it is suggested that $B_m < 0.2\,\Delta B_{pp}$ (*16*). Sensitivity optimization of CW EPR was carried out with imaging as the primary goal. The optimal value for modulation amplitude was selected in such a way that there is no spectral distortion. By varying the B_m it was found that maximum sensitivity, without any distortion in lineshape, could be achieved at $B_m \sim 0.3\,\Delta B_{pp}$. The limiting value of B_m becomes critical for narrow-line spin probes such as the triarylmethyl (TAM) radical (*18*). Therefore for narrow-line spin probes the pulsed method, which is free of any such constraint, is expected to give better sensitivity. However, line broadening caused by larger modulation amplitude may be modeled (*41*) and in such cases the sensitivity may be improved by an additional factor of 3.

In principle, it is possible to increase the peak-to-peak height of the EPR signal by increasing the filter time constant (i.e., decreasing the bandwidth) of the lock-in amplifier. But this in turn will require a long scan time, leading to a long image acquisition time, which will eventually be determined by the spin probe clearance rate and the required temporal resolution. When quantitative information is required, a time constant which is less than 1/10th of the time required to scan through the ΔB_{pp} field would result in distortion-free spectra. Under a gradient of 1 G/cm, for a full view of a 25 × 25 mm resonator, the scan width becomes 2.5 G. Hence a time constant of 0.03 s for a scan time of 2 s is close to the optimal value for the narrow-line spin probes.

III. EXPERIMENTAL

Pulsed EPR Spectrometer

The instrumentation of the 300-MHz pulsed EPR spectrometer and the details of the data acquisition system and resonators are described in earlier reports (*19, 21*). Since these earlier reports, the following modifications have been carried out to further enhance the capabilities of the pulsed RF EPR spectrometer. The local oscillator frequency was changed from 350 to 320 MHz, so that the center of the intermediate frequency is at 20 MHz, instead of 50 MHz. The diplexor was redesigned to further reduce the insertion loss and switching times and the

preamplifier was housed close to the diplexor in a shielded enclosure. With these alterations, an isolation of 30 dB between the transmit and receive arms is realized, compared to 25 dB prior to these changes. Additionally, a shielded enclosure was provided to the magnet/gradient assembly to minimize the RF noise from the environment. DC feed-through was a problem faced in the earlier configuration of the spectrometer. Even though the transmit RF is gated for the required pulse width, the 300-MHz carrier signal is persistent at all the time in the system. To eliminate this, one of the input signals was pregated. In our spectrometer, the main RF source is an 800-MHz crystal oscillator. From this master oscillator, frequency dividers generate a set of frequencies, namely 400, 200, 100, 50, 20, and 10 MHz. These frequencies were combined suitably to generate 500 and 320 MHz. All these frequencies maintain a definite phase relationship to the 800 MHz source. The 300 MHz was synthesized by mixing 800 and 500 MHz. The 500 MHz was pregated before mixing. The pregate pulse width was adjusted, taking into account the rise time of the 300-MHz filter. The gating time was adjusted so that the 300 MHz was available only for about 20 to 50 ns longer than the transmit pulse width. Hence until the receiver recovers, there will be no 300 MHz present anywhere in the system. In this manner the feedthrough was completely eliminated.

CW EPR Spectrometer

The design and construction of the CW 300-MHz EPR spectrometer were published recently (*8*) and the CW EPR measurements reported in the present study are made without any further change in the CW EPR spectrometer. Table 1 summarizes the important specifications of the two spectrometers.

TABLE 1

Specifications	Pulsed spectrometer	CW spectrometer
Frequency (MHz)	300	300
Microwave power (W)	70	0.008
Attenuation	0–60 dB in steps of 1 dB	0–60 dB in steps of 1 dB
Resonator	Parallel coil	Parallel coil
Efficiency parameter (mG/($\sqrt{}$W)	23	23
Loaded Q-factor	25	1800
90° Pulse width	90 ns	—
Dead time	275 ns	—
Detection arm	Quad detection	—
	500-MHz 8-bit digitizer	
	Record length up to 4 k	1 k
	Repetition rate 20 μs	4 s
Field modulation	—	0 to 4 G
Modulation frequency (kHz)	—	13.5
Minimum scan time	—	2 s
Preamp noise figure	0.8 dB	0.8 dB
Receiver dynamic range	60 dB	—

Resonators

A home-built parallel coil resonator (25 × 25 mm) was used for spectral measurements and imaging. Parallel coil resonators have been evaluated for their applications in pulsed RF EPR imaging (*21*). The Q of the resonator was adjusted to about 25 by a combination of both over-coupling and resistive damping for pulsed EPR studies to achieve optimal B_1 as well as minimal reflected power. For an input power of 64 dBm, the reflected power was measured to be about 3 dBm and the dead time of the spectrometer was 275 ns.

Spin Probes

The spin probes used for the pulsed EPR study are based on the triarylmethyl (TAM) skeleton; they are nontoxic, and water-soluble. Two analogs of TAM, abbreviated as Oxo31 and Oxo63, obtained from Nycomed Innovations, Malmo, Sweden, were used in this study. The structural details of these agents and their EPR properties are described elsewhere (*18*). Recently these spin probes have been evaluated as contrast agents for dynamic *in vivo* oxymetry using Overhauser enhanced MR imaging (*17*).

The EPRI experiments involving animals were performed in accordance with the guide for the care and use of laboratory animals prepared by the institute of laboratory animal resources, National Research Council. The details of animals and animal-handling protocols are described elsewhere (*20*). The imaging experiments were carried out per the procedure reported earlier (*19, 20*). The 2D images were obtained using filtered back-projection reconstruction techniques.

IV. PERFORMANCE EVALUATION

Spectroscopy

Figure 1 shows the spectra of three different free radicals measured at the limiting concentration with respect to sensitivity in detection. In order to compare the pulsed and CW methods one has to consider sensitivity per unit time. Hence the total measurement time was kept constant for all these measurements. With the rapid scan capability of the CW spectrometer, a sweep rate of 5 G/s could be implemented. Nevertheless to keep the spectral distortion at a minimum, we have used a scan time of 2 s for all these CW experiments. Consequently for the sake of comparison in the case of pulsed measurements, coherent averages were done for 2 s and the averaged FIDs were Fourier transformed to get the absorption mode spectra shown in Fig. 1. The spectra were recorded with 8 ml of the spin probe solution (65% filling factor). The SNR values obtained from the spectra of the two spin probes at various concentrations are plotted in Fig. 2. For an SNR of 1, the minimum detectable concentrations (N/V_S) have been computed and these values are given in Table 2A.

The expected ratio of sensitivity of the CW experiment to the pulsed experiment is given by (*26, 35*)

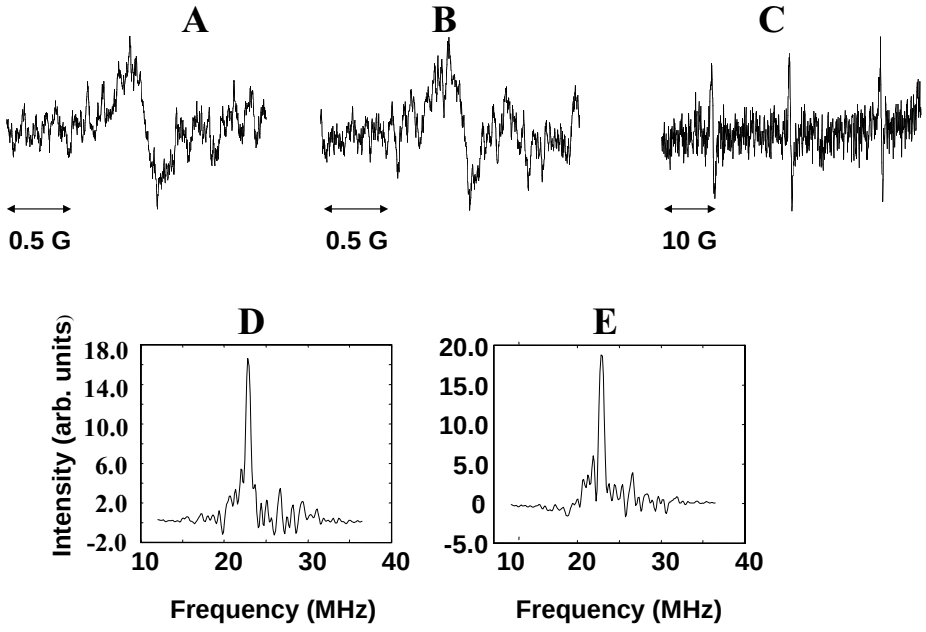

FIG. 1. The 300-MHz CW EPR spectra of an air-equilibrated solution of 10-μM Oxo63 (A), 5-μM Ox031 (B), and 10-μM tempone (C) in 8 ml of saline. The instrumental parameters for Oxo63 are sweep width, 2 G; scan time, 2 s; time constant, 0.03 s; modulation amplitude, 0.1 G; RF power, 2.25 mW. For Oxo31, sweep width, 2 G; scan time, 2 s; time constant, 0.03 s; modulation amplitude, 0.08 G; RF power, 2.25 mW. For tempone, sweep width, 50 G; scan time, 32 s; time constant, 0.03 s; modulation amplitude, 0.5 G; RF power, 2.25 mW. The corresponding 300-MHz pulsed EPR spectra are given in (D) Oxo63 and (E) Oxo31. The resonator $Q = 25$; RF pulse width = 90 ns; the sampling rate = 500 MS/s; number of averages = 100,000; acquisition time = 2 s.

$$(\mathrm{SNR})_{\mathrm{cw}}/(\mathrm{SNR})_{\mathrm{pulsed}} \propto \sqrt{(\delta f/\Delta f)} \times \sqrt{(T_1/t_{\mathrm{rep}})}. \qquad [18]$$

Here δf is the full linewidth at half-height of the resonance. The ratio, $\Delta f/\delta f$, gives the number of spectral elements present in a spectrum. For single-line spectra, this ratio is not a significant factor and hence the sensitivity advantage will depend mainly upon the speed of the data acquisition system. The spin–lattice relaxation times of the TAM radicals, T_1, are in the range of about 500 ns. With $T_1 = 500$ ns and $t_{\mathrm{rep}} = 5$ μs, the pulsed method is expected to show a sensitivity advantage by a factor of about 6, which compares reasonably well with the experimentally observed factor of about 4 (Table 2A). This observation of a sensitivity advantage of the pulsed technique is not surprising because uniform excitation of the entire spectrum is feasible for narrow line compounds. Also, the long relaxation time limits the loss in sensitivity arising due to the finite dead time of the spectrometer.

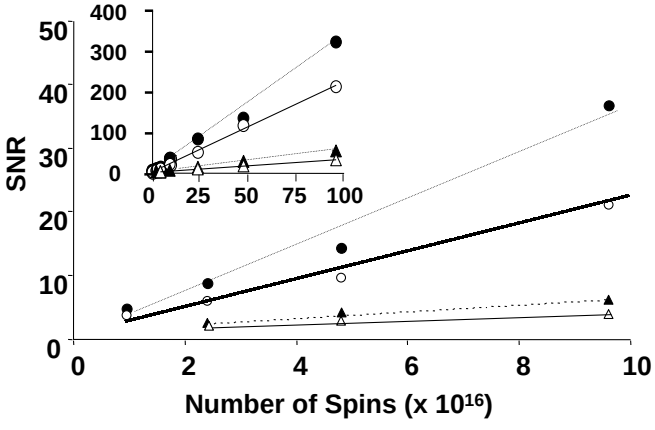

FIG. 2. Sensitivity comparison of CW and pulsed methods for different spin probes. △△△, Oxo63 CW; ▲▲▲, Oxo31 CW; ●●●, Oxo31 FT; and ○○○, Oxo63 FT methods. Inset shows the measurement at extended concentrations.

Imaging

The sensitivity advantage of the pulsed technique should be particularly pronounced for spectra with narrow resonance lines covering a wide spectral bandwidth. In an imaging experiment

TABLE 2A
Sensitivity Parameters

Technique	Spin probe	Linewidth (mG)[a]	SNR[b]	$N_{\mathrm{min}} \times 10^{15}$ (spins)[c]
Pulsed	Oxo31	160	14.3	0.96
	Oxo63	210	9.6	0.96
CW	Oxo31	180	3.4	2.4
	Oxo63	220	2.9	4.8
	Tempone	520	1.9	9.6

[a] Air-saturated, 20-μM solution.
[b] Resonator, parallel coil; size, 25 × 25 mm; 8-ml spin probe solution in PBS.
[c] Estimated for $\eta = 1$ and SNR = 1.

using a single 90° pulse, if all the spins can be excited simultaneously (satisfying Eq. [12]), then improvement in sensitivity per unit time on the order of $\sqrt{(\Delta f/\delta f)}$ could be achieved by the Fellgett advantage. In a typical experiment using a gradient of 1.0 G/cm, the Δf becomes 2.5 G for the (2.5 × 2.5)-cm parallel coil resonator. For trityl radicals, the improvement in sensitivity will be $\sim\sqrt{(2.5/0.2)} = 3.5$. However, imaging of a large object poses many problems as discussed earlier. The gradient-induced line-broadening limits the SNR of the projections in the pulsed method, because of the loss in the exponentially decaying FID, which in turn will limit the size of the object. With current technical specifications we have optimized the resonator size to be 25 × 25 mm and the gradient to be 0.5 G/cm. To assess the two techniques for their imaging capability, both phantom and animal imaging experiments were designed (Table 2B). Three holes (4-mm diameter) drilled in the Lucite cylinder were filled with 250 μl of the spin probe Oxo63 in different concentrations for phantom experiments. Figure 3 summarizes the results of phantom imaging.

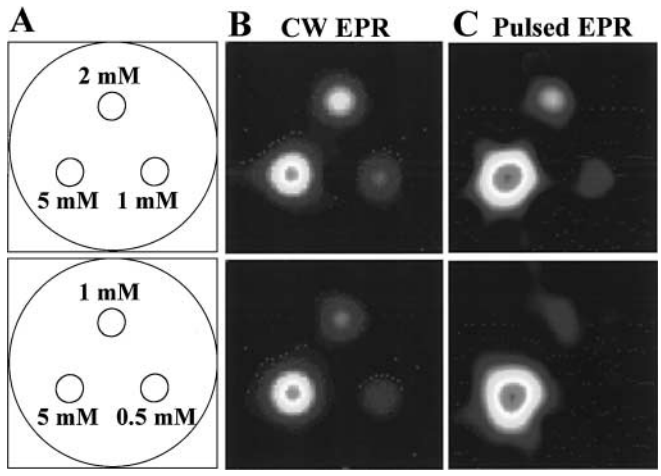

FIG. 3. Schematics of phantom (A) consisting of three tubes (i.d. 4 mm) containing Oxo63 at different concentrations. The center-to-center distance between the tubes is 14 mm. (B) The two-dimensional transverse image (field of view, 25 × 25 mm) of the phantom by 300-MHz CW EPR. Image data acquisition parameters: gradient strength, 0.8 G/cm; number of projections, 36 (1024 points each, with a single 2-s scan per projection); acquisition time, 1.8 min. Two-dimensional transverse image (field of view, 25 × 25 mm) of the phantom by 300 MHz pulsed EPR (C). Image data acquisition parameters: number of projections, 36; number of averages per projection, 100,000; gradient strength, 0.8 G/cm, acquisition time, 1.2 min. Record length per FID, 4K points at a sampling rate of 500 MS/s.

Image Uniformity

Uniformity of an image is achieved from the variation of the image signal intensity over the region of interest (ROI) of an object of uniform spin density. Some factors that can affect the image uniformity are inhomogeneities in the Zeeman field, nonlinearity in gradients, nonuniform RF flux, and response of the receiver system. The magnet system and the gradient assembly used are the same for both the pulsed and CW spectrometers. Therefore, the difference in image quality in the pulsed technique, if any, may originate mainly from the nonuniform RF flux and the receiver response.

Figures 3B and 3C show the transverse 2D spatial images of the phantom obtained by the CW and pulsed methods, respectively. The CW technique shows fairly good image uniformity. On the other hand the pulsed technique shows some distortion that may be attributed to several factors. An FOV of 25 mm under a gradient of 0.5 G/cm corresponds to a Δf of 3.5 MHz. According to Eq. [12], this translates into a $t_p(90°)$ of about 70 ns. However, with the current configuration of our pulsed system, $t_p(90°)$ is about 90 ns. Hence, as discussed earlier, incomplete excitation may lead to spectral distortions. Pulse shaping, resonators of high efficiency parameter, Λ, and high transmit power may help to solve this problem. Second, the Q-factor of the resonator causes the RF power profile to droop at either extreme of the spectral window. This in turn will cause a reduction in the intensity of spectral features as a function of offset frequency. The narrow-band detection scheme of the CW EPR technique alleviates this problem. Third, the T_2^* of the FIDs will depend on the spectral range. Thus for orientation of the gradient vector along the axis of a cylindrical distribution of spins, the T_2^* will be shorter than for the perpendicular direction. This will lead to a differential loss in integrated intensity among the various projections, causing artifacts in the back-projected image (*20*).

Additionally, this phantom imaging also brings out the dynamic range of spin probe detection by the two techniques. Figures 3B and 3C show that CW EPRI could easily discern regions having 10 times lower spin content in the field of view; in FT EPRI has limited dynamic range discrimination. This may pose problems if the spin probe localizes selectively in a particular organ (such as the bladder) while whole-body imaging is performed.

TABLE 2B
Specifications for Imaging[a]

	CW	Pulsed[b]
Acquisition time		
2D (18 projections)	54 s	20 s
3D (81 projections)	4 min	1.5 min
Spin probes	Oxo63, Oxo31, Nitroxide	Oxo63, Oxo31
Maximum gradient (G/cm)	5	0.8
Maximum object size (cm × cm)	5 × 3	5 × 2.5

[a] Optimized for small animal imaging.
[b] Number of averages per projection, 50,000.

Spatial Resolution

This is one of the most important parameters of an imaging system, because it characterizes the capacity of the system to make fine details visible. In a digital image, the resolution is

pixel-limited. This theoretical limit may be simply estimated from the pixel size. For a 2D image of area a^2 and resolution x, the number of pixel elements required, N, is given by

$$N = \{a/x\}^2. \quad [19]$$

In vivo pulsed EPR imaging reported in this study is done using a parallel coil resonator of size 25 × 25 mm and a gradient of 0.5 G/cm, corresponding to a spectral width of 1.25 G. The 2D image given in Fig. 5 is of dimension 64 × 64, corresponding to a pixel-limited resolution of 0.4 mm. However, the linewidth-limited resolution, Δz, is given by

$$\Delta z = \Delta B/G_Z. \quad [20]$$

Here G_Z is the gradient applied along the direction of the samples and ΔB is the linewidth of the spin probe. The linewidths of the various spin probes used in the present study are listed in Table 2A. One can use a larger gradient for better resolution, but the gradient-induced line broadening will compromise the SNR because of the spectrometer dead time in FT EPRI. In contrast, for the CW method there is no detection problem even for very large gradients. Therefore, the CW method has the potential for better resolution, although microwave power saturation and modulation broadening may pose problems when narrow-line spin probes are used. The gradient amplitude used in the present study was limited mainly because of the problems associated with the pulse technique rather than the CW method. Hence an optimal gradient of 0.5 G/cm was selected for the pulsed EPR studies, although the gradient assembly of the imager can provide a maximum gradient of 5 G/cm.

The resolution expected from a pulsed EPR image can be estimated by

$$\Delta x = 2/(\gamma_e G_z T_2^*), \quad [21]$$

where T_2^* is the spin–spin relaxation time under the influence of the gradient. The optimal acquisition time of each FID is related to T_2^* and may be approximated by

$$T_{\text{acq}} = 2\pi/\gamma \Delta B_{pp} = \pi T_2^*. \quad [22]$$

Under the present acquisition conditions, the resolution for a gradient of 0.5 G/cm is estimated to be about 1.8 mm. The results of phantom imaging indicate an approximate resolution of 2 mm, in accordance with this expectation.

Yet another factor that severely limits the spatial resolution is the sensitivity of the spectrometer/imager. It is essential that the pixel contain enough spins to be detectable by the spectrometer. Hence based on this $N_{\min}$ value, one has to select an optimal concentration of the spin probe. For a 3D image with resolution x, the sensitivity-limited resolution is given by

$$x^3\rho = N_{\min}, \quad [23]$$

where ρ is the mean spin density. It may appear that the resolution can be improved by increasing the concentration of the spin probe. But for *in vivo* imaging, both line broadening due to spin–spin interaction and toxicity of the spin probe will limit the dose of the spin probe. For the TAM spin probes, toxicity studies in small animals (rats and mice) show the safe dose to be about 1.8 g per kg of body weight (~2.5 mM/kg) (*17*), leading to a ρ value of 6.02×10^{17} spins/cc. Hence for small-animal imaging using TAM spin probes, the sensitivity-limited resolution of the pulsed RF EPR imager is 2.6 mm.

Temporal Resolution

For reliable interpretation of the EPR image data, the exogeneously administered spin probe must be stable *in vivo* until the imaging protocol is completed. In addition to spatial information of free radical distribution, physiological information such as oxygen concentration can also be obtained from EPRI. Reduced data acquisition time enables examination of temporal changes both in the spin probe and in the oxygen distribution at the rate comparable to the clearance of the spin probe. EPRI can also be used to study kinetics of metabolic changes of the exogenous spin probe such as nitroxides *in vivo* (*42*). The speed of the image data acquisition system is very crucial for the success of these studies. In our pulsed system, a 2D data set consisting of 18 projections (each of 4K samples and 50,000 averages) can be acquired, using the current configuration of the imager, within about 20 s. Similarly, a 3D data set of 81 projections can be collected within 90 s. The corresponding times for the CW imaging are 54 s and 4 min, respectively.

In Vivo Imaging

Figure 4 shows a sequence of 2D CW EPR images of Oxo-63 distribution in an anesthetized mouse after intravenous administration. The mouse was positioned (A) in the resonator in such a manner that the thoracic, abdominal, and pelvic regions were in the FOV. Projections corresponding to 2D images were collected at 2.8, 9.0, 13.0, and 16.9 min (B, C, D, E, respectively) after spin probe administration using a gradient of 1.0 G/cm. The image at the first time point was interpreted as spin probe localization predominantly in the two kidneys with some intensity in other organs in the abdominal region such as the liver and spleen. Subsequent images suggest a progressive redistribution of the spin probe from the circulation to the bladder as evidenced by the increasing image intensity from the bladder. However, contours corresponding to the two kidneys could be seen even in the presence of an intense signal from the bladder. The physical dimensions of the organs obtained from the EPR images were in good agreement with the actual dimensions. Figure 4F shows a graph of the decrease in the average spin count from the kidneys and the increase in the spin count in the bladder as a function of time.

Figure 5 shows 2D images of the spin probe Oxo63 distribution obtained by FT EPRI after intravenous administration in a

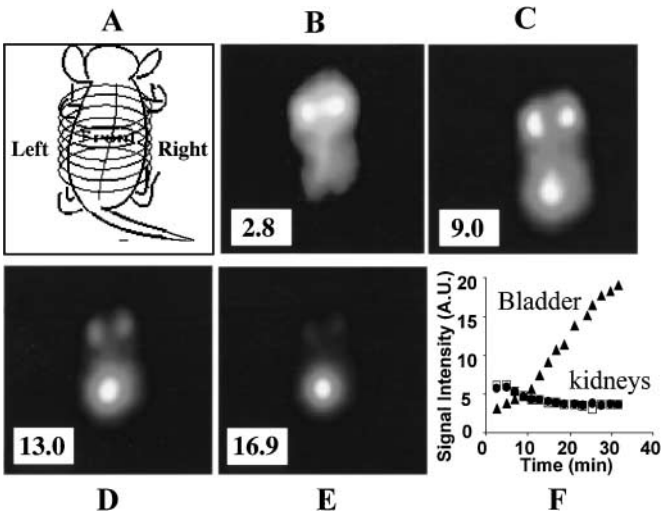

FIG. 4. The 2D CW EPR images of a C3H mouse taken as a function of time from the infusion of Oxo63 via tail-vein cannulation and the visualization of the clearance of the spin probe. The cartoon shows the position of the mouse (A). The images (B to E) show progressive accumulation of the spin probe in the bladder. The time course of the spin probe in various organs (□, left kidney; ●, right kidney; ▲, bladder) was computed by selecting the corresponding regions in the sequential images and averaging the pixel intensities. Image acquisition parameters: gradient strength, 1 G/cm; number of projections, 18 (512 points each, with a single 4-s scan per projection); acquisition time, 1.5 min.

mouse as a function of time. The images were taken at 3, 6, 9, and 12 min after spin probe administration using a magnetic field gradient of 0.5 G/cm. Again, as in the case of CW EPR imaging experiments, in the initial image a predominant distribution of the spin probe was seen in the kidneys. Subsequent images show a progressive decrease in intensity of the spin probe in the kidneys with a corresponding increase in the bladder. However, unlike the case of CW EPR images (Fig. 4), the image intensity from the bladder overwhelmed the intensity from the kidney and other regions, because of dynamic range problems mentioned earlier.

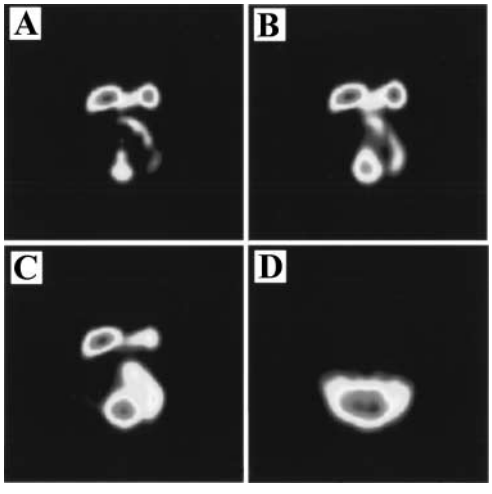

FIG. 5. The 2D pulsed EPR image of a C3H mouse showing the kidneys and the bladder in an experiment analogous to the one described in Fig. 4. Image acquisition parameters: number of projections, 36; number of averages per projection, 50,000; gradient strength, 0.5 G/cm; acquisition time, 36 s. Record length per FID, 4K points at a sampling rate of 500 MS/s. Images A, B, C, D were taken at 3, 6, 9, and 12 min after the infusion of spin probe Oxo63. Just as in the CW images, one can see a gradual increase in the spin count in the kidney.

V. DISCUSSION

Development of EPR instrumentation for biological applications has continued to be a challenging task (*3, 6, 40, 43, 44*). Although a commercial L-band imaging system has now become available (*45*), specialized instrumentation is still required for many applications. We have shown that both pulsed and CW RF spectrometers could be constructed with many commercially available modules (*8, 46*). In this communication, a comparison of these two spectrometers is presented, pointing out their potential and limitations, so that application scientists can make a choice of the technique based on need. The performance evaluation reported is based only on the existing configuration of the spectrometers. Additional improvements to the existing system are possible and these are outlined below.

In its current configuration, the CW spectrometer operates only with an automatic frequency control. Although reasonable sensitivity and minimal motion artifacts are realized, implementation of automatic coupling control will improve the quality of projections by compensating for changes in the resonator impedance induced by animal motion. Similarly, implementation of automatic phase control (APC) can enhance the SNR, because the phase error can have a marked effect on the noise level (*13*). Hence APC can particularly improve the consistency of the projections of large size objects in lengthy 3D data acquisition schemes. Also the temporal resolution can be improved by the addition of the rapid scan facility (*47*).

The rectangular pulses employed in our study have a $(\sin x)/x$ power profile. Therefore, while the spectral coverage at the center is flat, the amplitude falls off rapidly at either end. This leads to intensity attenuation in the image profiles, especially in large objects and/or at large gradients. In MRI, a fairly accurate slice selection is carried out using a $(\sin x)/x$ pulse with 1–2 side lobes. While a slice selection strategy may not be feasible in FT EPR, use of a shaped pulse for the RF excitation can improve the quality of the pulsed EPR images. Also in the pure phase encoding imaging modality such as constant time imaging may improve the quality of the pulsed EPR images significantly (*48*). Our initial experiments in this direction have provided very promising results.

The potential of EPRI for functional imaging has been recognized (*49*). EPR can provide useful pathophysiological and biophysical information because of the capabilities of ESR spectra to reflect the environmental conditions. For example, it is possible to study the tissue metabolic redox state (*50*), to monitor pO_2 in normal and tumor tissues (*43*) and to measure tissue pH and

viscosity (*7*). Also, short-lived radical species can be detected indirectly by *in vivo* spin trapping (*51*). However, the linewidths of nitroxides and the spin adducts of biological interest preclude their detection by the pulsed technique. Hence the CW technique has an edge over the pulsed technique for the study of these large-linewidth systems. Nevertheless, the recent development of narrow-line spin probes for functional imaging (*18*) and the potential of the pulsed technique to provide better sensitivity and temporal resolution for such narrow-line spin probes hold attraction for the development of low-frequency pulsed EPR instrumentation. The possibility of coregistering anatomic images (MRI) with functional images (EPRI) (*52–54*) is likely to add extra impetus to research in this field.

REFERENCES

1. G. He, R. A. Shankar, M. Chzhan, A. Samouilov, P. Kuppusamy, and J. L. Zweier, Noninvasive measurement of anatomic structure and intraluminal oxygenation in the gastrointestinal tract of living mice with spatial and spectral EPR imaging, *Proc. Natl. Acad. Sci. U.S.A.* **96,** 4586–4591 (1999).
2. G. M. Rosen, S. Pou, H. J. Halpern, T. I. Smirnova, A. I. Smirnov, R. B. Clarkson, and R. L. Belford, In vivo detection of free radicals in real time by low-frequency electron paramagnetic resonance spectroscopy, *Methods Mol. Biol.* **108,** 27–35 (1998).
3. H. M. Swartz and T. Walczak, Developing in vivo EPR oximetry for clinical use, *Adv. Exp. Med. Biol.* **454,** 243–252 (1998).
4. P. Kuppusamy, R. A. Shankar, V. M. Roubaud, and J. L. Zweier, Whole body detection and imaging of nitric oxide generation in mice following cardiopulmonary arrest: Detection of intrinsic nitrosoheme complexes, *Magn. Reson. Med.* **45,** 700–707 (2001).
5. T. Yoshimura, H. Yokoyama, S. Fujii, F. Takayama, K. Oikawa, and H. Kamada, In vivo EPR detection and imaging of endogenous nitric oxide in lipopolysaccharide-treated mice, *Nat. Biotechnol.* **14,** 992–994 (1996).
6. M. C. Krishna, N. Devasahayam, J. A. Cook, S. Subramanian, P. Kuppusamy, and J. B. Mitchell, Electron paramagnetic resonance for small animal imaging applications, *Ilar J.* **42,** 209–218 (2001).
7. H. J. Halpern, G. V. R. Chandramouli, C. Yu, M. Peric, E. Barth, B. A. Teicher, and D. Grdona, Pharmacological compartment viscosity and polarity measured with very low-frequency EPR in tumors of living animals, *Magn. Reson. Chem.* **33,** 147–153 (1995).
8. J. Koscielniak, N. Devasahayam, M. S. Moni, P. Kuppusamy, K. Yamada, J. B. Mitchell, M. C. Krishna, and S. Subramanian, 300 MHz continuous wave electron paramgnetic resonace spectrometer for small animal *in vivo* imaging, *Rev. Sci. Instrum.* **71,** 4273–4281 (2000).
9. J. A. Brivati, A. D. Stevens, and M. C. R. Symons, A radiofrequency ESR spectrometer for in vivo imaging, *J. Magn. Reson.* **92,** 480–489 (1991).
10. D. Dijret, M. Beranger, A. Bernerd, C. Jeandey, and M. Moussavi, A new 280-MHz ESR spectrometer, *J. Chim. Phys. Phys.-Chim. Biol.* **91,** 1862–1867 (1994).
11. H. J. Halpern, D. P. Spencer, J. Van Polen, M. K. Bowman, A. C. Nelson, E. M. Dowey, and B. A. Teicher, Imaging radio frequency electron-spin resonance spectrometer with high resolution and sensitivity for in vivo measurements, *Rev. Sci. Instrum.* **60,** 1040–1050 (1989).
12. M. Alecci, S. D. Penna, A. Sotgiu, L. Testa, and I. Vannucci, Electron paramagnetic resonance spectrometer for three-dimensional in vivo imaging at very low frequency, *Rev. Sci. Instrum.* **63,** 4263–4270 (1992).
13. A. D. Stevens and J. A. Brivati, A 250 MHz EPR spectrometer with rapid phase-error correction for imaging large biological specimens, *Meas. Sci. Technol.* **5,** 793–796 (1994).
14. M. Decorps and C. Fric, Un spectrometre basse frequence a haute sensibilite pour l'etude de la resonance des spins electroniques, *J. Phys. E* **5,** 337–342 (1972).
15. V. Quaresima and M. Ferrari, Current status of electron spin resonance (ESR) for in vivo detection of free radicals, *Phys. Med. Biol.* **43,** 1937–1947 (1998).
16. A. I. Smirnov, S. W. Norby, T. Walczak, K. J. Liu, and H. M. Swartz, Physical and instrumental considerations in the use of lithium phthalocyanine for measurements of the concentration of the oxygen, *J. Magn. Reson. B* **103,** 95–102 (1994).
17. K. Golman, J. S. Petersson, J. H. Ardenkjaer-Larsen, I. Leunbach, L. G. Wistrand, G. Ehnholm, and K. Liu, Dynamic in vivo oxymetry using overhauser enhanced MR imaging, *J. Magn. Reson. Imaging* **12,** 929–938 (2000).
18. J. H. Ardenkjaer-Larsen, I. Laursen, I. Leunbach, G. Ehnholm, L. G. Wistrand, J. S. Petersson, and K. Golman, EPR and DNP properties of certain novel single electron contrast agents intended for oximetric imaging, *J. Magn. Reson.* **133,** 1–12 (1998).
19. R. Murugesan, J. A. Cook, N. Devasahayam, M. Afeworki, S. Subramanian, R. Tschudin, J. A. Larsen, J. B. Mitchell, A. Russo, and M. C. Krishna, In vivo imaging of a stable paramagnetic probe by pulsed-radiofrequency electron paramagnetic resonance spectroscopy, *Magn. Reson. Med.* **38,** 409–414 (1997).
20. M. Afeworki, G. M. van Dam, N. Devasahayam, R. Murugesan, J. Cook, D. Coffin, J. H. Larsen, J. B. Mitchell, S. Subramanian, and M. C. Krishna, Three-dimensional whole body imaging of spin probes in mice by time-domain radiofrequency electron paramagnetic resonance, *Magn. Reson. Med.* **43,** 375–382 (2000).
21. N. Devasahayam, S. Subramanian, R. Murugesan, J. A. Cook, M. Afeworki, R. G. Tschudin, J. B. Mitchell, and M. C. Krishna, Parallel coil resonators for time-domain radiofrequency electron paramagnetic resonance imaging of biological objects, *J. Magn. Reson.* **142,** 168–176 (2000).
22. M. Alecci, J. A. Brivati, G. Placidi, and A. Sotgiu, A radiofrequency (220-MHz) Fourier transform EPR spectrometer, *J. Magn. Reson.* **130,** 272–280 (1998).
23. A. Feintuch, G. Alexandrowicz, T. Tashma, Y. Boasson, A. Grayevsky, and N. Kaplan, Three-dimensional pulsed ESR Fourier imaging, *J. Magn. Reson.* **142,** 382–385 (2000).
24. A. Coy, N. Kaplan, and P. T. Callaghan, Three-dimensional pulsed ESR imaging, *J. Magn. Reson. A* **121,** 201–205 (1996).
25. P. P. Borbat, R. H. Crepeau, and J. H. Freed, Multifrequency two-dimensional Fourier transform ESR: An X/Ku-band spectrometer, *J. Magn. Reson.* **127,** 155–167 (1997).
26. T. F. Prisner, M. Rohrer, and K. Mobius, Pulsed 95 GHz high field EPR heterodyne spectrometer with high spectral and time resolution, *Appl. Magn. Reson.* **7,** 167–183 (1994).
27. G. A. Rinard, R. W. Quine, S. S. Eaton, G. R. Eaton, and W. Froncisz, Relative benefits of overcoupled resonators vs inherently low-Q resonators for pulsed magnetic resonance, *J. Magn. Reson. A* **108,** 71–81 (1994).
28. S. Van Doorslaer, G. A. Sierra, and A. Schweiger, Dead time-dependent line distortions in absolute-value electron spin echo envelope modulation spectra, *J. Magn. Reson.* **136,** 152–158 (1999).
29. D. Hessinger, C. Bauer, M. Hubrich, G. Jeschke, and H. W. Spiess, Magic-angle sample spinning electron paramagnetic resonance–instrumentation, performance, and limitations, *J. Magn. Reson.* **147,** 217–225 (2000).
30. S. Derek, "Fourier Transform N.M.R. Spectroscopy," Elsevier, Amsterdam (1984).
31. C. M. Lai and P. C. Lauterbur, Automatic correction of nuclear magnetic resonance zeugmatographic projections, *J. Phys. E* **14,** 874–879 (1981).
32. H. Barkhuijsen, R. De Beer, and D. Van Ormondt, Improved algorithm for noniterative time-domain model fitting to exponentially damped magnetic resonance signals, *J. Magn. Reson.* **73,** 553–557 (1987).

33. D. O. Kuethe, A. Caprihan, I. J. Lowe, D. P. Madio, and H. M. Gach, Transforming NMR data despite missing points, *J. Magn. Reson.* **139,** 18–25 (1999).

34. R. R. Ernst, Magnetic resonance with stochastic excitation, *J. Magn. Reson.* **3,** 10–27 (1970).

35. R. R. Ernst, G. Bodenhausen, and A. Wokaun, "Principles of Nuclear Magnetic Resonance in One and Two Dimensions," Oxford Univ. Press, New York (1987).

36. L. Kevan and M. K. Bowman, "Modern Pulsed and Continuous-Wave Electron Spin Resonance," Wiley, New York (1990).

37. G. A. Rinard, R. W. Quine, J. R. Harbridge, R. Song, G. R. Eaton, and S. S. Eaton, Frequency dependence of EPR signal-to-noise, *J. Magn. Reson.* **140,** 218–227 (1999).

38. G. R. Eaton, S. S. Eaton, and G. A. Rinard, Frequency dependence of EPR sensitivity, *in* "Spatially Resolved Magnetic Resonance" (P. Blumler, B. Blumich, R. Botto, and E. Fukushima, Eds.), pp. 65–74, Wiley–VCH, Weinheim (1998).

39. E. D. Becker, Introduction to pulse and fourier transform methods, *in* "Nuclear Magnetic Resonance Spectroscopy of Nuclei Other Than Protons" (T. Axenrod and G. A. Webb, Eds.), pp. 17–29, Wiley, New York (1974).

40. A. J. Hoff, "Advanced EPR: Applications in Biology and Biochemistry," Elsevier, Amsterdam (1989).

41. B. H. Robinson, C. Mailer, and A. W. Reese, Linewidth analysis of spin labels in liquids. I. Theory and data analysis, *J. Magn. Reson.* **138,** 199–209 (1999).

42. N. Phumala, T. Ide, and H. Utsumi, Noninvasive evaluation of in vivo free radical reactions catalyzed by iron using in vivo ESR spectroscopy, *Free Radical Biol. Med.* **26,** 1209–1217 (1999).

43. P. Kuppusamy, M. Afeworki, R. A. Shankar, D. Coffin, M. C. Krishna, S. M. Hahn, J. B. Mitchell, and J. L. Zweier, In vivo electron paramagnetic resonance imaging of tumor heterogeneity and oxygenation in a murine model, *Cancer Res.* **58,** 1562–1568 (1998).

44. H. Fujii and L. J. Berliner, Ex vivo EPR detection of nitric oxide in brain tissue, *Magn. Reson. Med.* **42,** 599–602 (1999).

45. "ELEXSYS E540: The L-Band Spectrometer for EPR Imaging," BRUKER Instruments, Inc., Billerica, MA 01821.

46. R. Murugesan, M. Afeworki, J. Cook, N. Devasahayam, R. Tschudin, J. B. Mitchell, S. Subramanian, and M. C. Krishna, A broadband pulsed radio frequency electron paramagnetic resonance spectrometer for biological applications, *Rev. Sci. Instrum.* **69,** 1869–1876 (1998).

47. H. Yokoyama, T. Ogata, N. Tsuchihashi, M. Hiramatsu, and N. Mori, A spatiotemporal study on the distribution of intraperitoneally injected nitroxide radical in the rat head using an in vivo ESR imaging system, *Magn. Reson. Imaging* **14,** 559–563 (1996).

48. S. Choi, X. W. Tang, and D. G. Cory, Constant time imaging approaches to NMR microscopy, *Int. J. Imag. Syst. Tech.* **8,** 263–276 (1997).

49. M. C. Krishna, S. Subramanian, P. Kuppusamy, and J. B. Mitchell, Magnetic resonance imaging for in vivo assessment of tissue oxygen concentration, *Seminar Radiat. Oncol.* **11,** 58–69 (2001).

50. B. Gallez, G. Bacic, F. Goda, J. Jiang, J. A. O'Hara, J. F. Dunn, and H. M. Swartz, Use of nitroxides for assessing perfusion, oxygenation, and viability of tissues: In vivo EPR and MRI studies, *Magn. Reson. Med.* **35,** 97–106 (1996).

51. H. J. Halpern, C. Yu, E. Barth, M. Peric, and G. M. Rosen, In situ detection, by spin trapping, of hydroxyl radical markers produced from ionizing radiation in the tumor of a living mouse, *Proc. Natl. Acad. Sci. U.S.A.* **92,** 796–800 (1995).

52. S. Di Giuseppe, G. Placidi, and A. Sotgiu, New experimental apparatus for multimodal resonance imaging: Initial EPRI and NMRI experimental results, *Phys. Med. Biol.* **46,** 1003–1016 (2001).

53. I. Nicholson, F. J. Robb, S. J. McCallum, A. Koptioug, and D. J. Lurie, Recent developments in combining LODESR imaging with proton NMR imaging, *Phys. Med. Biol.* **43,** 1851–1855 (1998).

54. T. Sato, K. Oikawa, H. OhyaNishiguchi, and H. Kamada, Development of an L-band electron spin resonance proton nuclear magnetic resonance imaging instrument, *Rev. Sci. Instrum.* **68,** 2076–2081 (1997).